UDC 621.313 https://doi.org/10.20998/2074-272X.2026.3.04

S. Shlyk, J. Pyrhönen, I. Petrov, M. Parviainen, I. Martikainen, A. Suikki, J. Pippuri-Mäkeläinen, M. Zagirnyak

Possibility of cooling the rotor of an electric traction motor by bidirectional air flows

Introduction. *The performance reliability of electric vehicles (EVs) is an important factor in evaluating their suitability for widespread adoption. The reliability and lifespan of an EV depend on several critical factors including the motor, battery pack, controllers, and thermal management systems. The* ***problem*** *addressed in this paper is to cool down the rotor of permanent magnet synchronous motor efficiently using new combined cooling methods.* ***Goal.*** *Determination of the effectiveness of the combined rotor cooling method, which includes a bidirectional airflow circulating through a designed fan and oil circulation in the hollow shaft.* ***Methodology.*** *The solution was carried out using CFD (computational fluid dynamics) analysis.* ***Results.*** *A numerical model of a new combined cooling method for the rotor, which taking into account heat generation in the rotor and the thermal influence of the stator and bearing units, based on heat flow equations that consider its laminar or turbulent nature, was developed and studied.* ***Scientific novelty.*** *Based on the analysis of the rotor's numerical model, a fan design was proposed that allows for effective heat dissipation by creating bidirectional airflow circulation.* ***Practical value.*** *The developed model can be used for further research on the dynamic thermal parameters of the rotor and evaluation of heat dissipation efficiency, which will optimize the heat and mass transfer processes within the motor, enhance its operational efficiency, and ensure the stability of its performance in various operating modes.* References 21, tables 5, figures 17.

Key words: **permanent magnet synchronous motor, combined cooling method, computational fluid dynamics, fan design, hollow shaft.**

Вступ. *Надійність роботи електромобілів (ЕМ) є важливим фактором в оцінці їх придатності для широкого впровадження. Надійність та термін служби ЕМ залежать від кількох критичних факторів, включаючи двигун, акумуляторну батарею, контролери та системи теплового управління.* ***Проблема,*** *що розглядається в цій статті, полягає в ефективному охолодженні ротора синхронного двигуна з постійними магнітами за допомогою нових комбінованих методів охолодження.* ***Мета.*** *Визначення ефективності комбінованого методу охолодження ротора, який включає двонаправлений потік повітря, що циркулює за допомогою розробленого вентилятора, та циркуляцію масла в порожнистому валу.* ***Методологія.*** *Розв'язання проблеми було проведено за допомогою CFD (обчислювальної гідродинаміки) аналізу.* ***Результати.*** *Розроблено та досліджено числову модель нового комбінованого методу охолодження ротора, яка враховує тепловиділення в роторі та температурний вплив статора та підшипникових вузлів, на основі рівнянь теплового потоку, що враховують його ламінарну або турбулентну природу.* ***Наукова новизна****. На основі проведеного аналізу числової моделі ротора запропоновано дизайн вентилятора, що дозволяє ефективно відводити тепло завдяки створенню двонаправленої циркуляції повітря.* ***Практична цінність.*** *Отримана модель може бути використана для подальшого дослідження динамічних теплових параметрів ротора та оцінці ефективності відведення тепла, що дозволить оптимізувати процеси тепломасообміну всередині двигуна, підвищити ефективність його роботи та забезпечити стабільність його функціонування в різних режимах експлуатації.* Бібл. 21, табл. 5, рис. 17.

Ключові слова: **синхронний двигун з постійними магнітами, комбінований метод охолодження, обчислювальна гідродинаміка, дизайн вентилятора, порожнистий вал.**

Introduction. Vehicle regulation in the EU favors vehicles that emit no or low pollutants and CO_2. Curbing vehicle emissions and improving vehicle efficiency to meet these regulatory requirements need multi-prong technical solutions of electric vehicles such as hybrid electric vehicles, plug-in hybrid electric vehicles, extended range electric vehicles and battery electric vehicles [1].

Present-day electric traction motors rely heavily on the use of rare-earth permanent magnets (PMs) that contain scarce elements like Neodymium and Dysprosium. This dependence is understandable from the perspective of energy efficiency and torque density, but it also introduces several challenges. First, these materials are imported into the EU and are costly. Second, rare earth elements are finite resources, and increasing demand may lead to a supply shortage or even deplete these resources in the future. The number of electric cars produced annually is in the range of 90 million, and heavy vehicles are 20 million. Therefore, one can foresee that if rare earths are used wastefully, the global resources will not be rich enough.

Consequently, more and more research is dedicated to development of new generation of high-speed synchronous reluctance motors with minimal usage of PM. It will allow reduced dependence on rare-earth PM materials while simultaneously enhancing their recyclability.

Problem statement. During the design of high-speed high-specific-power motors, researchers face the significant problem that increased motor loss density results in very challenging heat dissipation. Heat generated during operation does not only have a negative effect on motor efficiency, but could lead to failure such as too high operating temperature of the motor, degrading of winding insulation, demagnetization of rotor magnets, eventual shorts, etc. [2−4]

In [5, 6] it is shown that approximately 75 % of motor performance problems are localized in the stator coil winding and rotor bars, which are most affected by temperature changes and mechanical stress. Internal losses (conduction losses, stator core losses, rotor core losses, and PM eddy current losses) and high temperatures affect the torque/rotational speed of the electric motor.

Reducing the temperature rise can happen by improving the cooling capacity of motor and by decreasing the losses.

Nowadays, there are a wide range of methods used for motor cooling. Depending on using different cooling media and materials with high thermal conductivity, they can be divided into 6 groups such as air cooling, liquid cooling, cooling using heat pipe, potting cooling, cooling using phase change materials, other cooling methods. Many studies have been conducted regarding the advantages and disadvantages of various cooling methods [7−10]. Nevertheless, there is currently no universally effective method for cooling the rotor. That is why it is essential to develop and evaluate new cooling approaches to ensure optimal performance and reliability of the rotor.

According to [11] one of the most effective cooling methods is liquid cooling. Due to the high specific heat capacity of liquids, this type of cooling allows absorbing and transferring significant amounts of heat. Nevertheless, such a cooling system requires additional equipment like pumps, heat exchangers, and valves, which can

complicate the system and increase the mass of it. Moreover, not only does the cost of system increase, but also the electricity consumption for operating components such as pumps also rises.

In contrast to liquid cooling, air cooling has less cooling performance, but it is much cheaper solution and does not require any additional equipment (except fan for forced cooling).

In this paper, the combined cooling method has been chosen to include both liquid and air cooling to evaluate effectiveness of this approach and its impact on internal temperatures within the motor [12].

The **goal of the work** is to determine the effectiveness of the combined rotor cooling method, which includes a bidirectional airflow circulating through a designed fan and oil circulation in the hollow shaft.

Materials and methods. The rotor was chosen as the object of cooling because, after the stator, it is the second location where significant amounts of heat are generated in the motor. The rotor with PMs of 120 kW motor is investigated (Fig. 1).

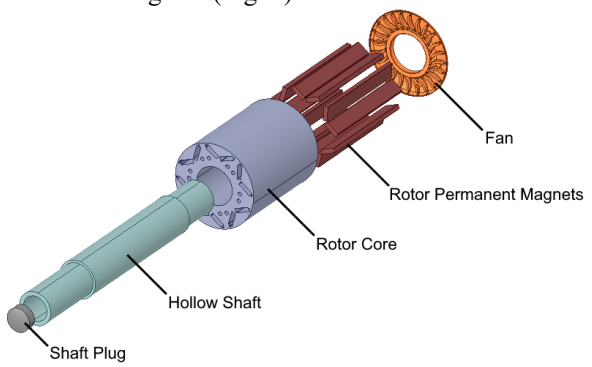

Fig. 1 Exploded view of the traction motor rotor unit

The rotor diameter is 86 mm and its active length is 110 mm. Magnets are buried inside the rotor in single layer «V» arrangement. The hollow shaft is cooled down by oil. In addition, the impeller fan is designed (Fig. 2) to provide cooling the rotor surface. It intakes air from the middle area of the PM V and blows it through the outer ends of the V-poles channels. The air heated close to the rotor surface should be cooled when colliding to the bearing shield cooled by bearing lubrication oil and cooled further in the inner duct of the rotor next to the well-cooled rotor shaft.

For air cooling of the rotor, an impeller fan is used (Fig. 2), which allows the creation of bidirectional airflow. Air is taken and pumped out in a volume of air limited by the inner wall of the stator, the outer surface of the left bearing shield, the front end of the rotor and the outer surface of the shaft.

It is assumed that the rotor is cooled by air due to the air passing through the internal channels of the rotor and its subsequent passage through the peripheral channels passing near the PMs (Fig. 3). The key factor in air cooling of the rotor is the transfer of its heat by air from the peripheral zones to the central part, where the heat is removed due to heat exchange between the hollow shaft and the oil circulating inside it. In this case, the degree of heat transfer coefficient (HTC) between the inner wall of the shaft and the oil is important.

In order to solve the equation of heat conduction, correct definitions of the initial and boundary conditions are required. The biggest research problem arises in the determination of the local heat transfer coefficient on the cooled surface. The heat conduction model based on the solution of the heat conduction equation in cylindrical coordinates with the use of numerical simulation methods was proposed in [10, 11]:

$$\lambda\left[\frac{\partial^2 T}{\partial r^2}+\frac{1}{r}\frac{\partial T}{\partial r}+\frac{\partial^2 T}{\partial z^2}\right]=\rho c\frac{\partial T}{\partial \tau}-q(r,z), \qquad (1)$$

where λ is the thermal conductivity; T is the temperature; r, z are the cylindrical coordinates; ρ is the density of the transmission medium; c is the heat capacity; τ is the time; q is the volumetric heat generation rate in the rotor.

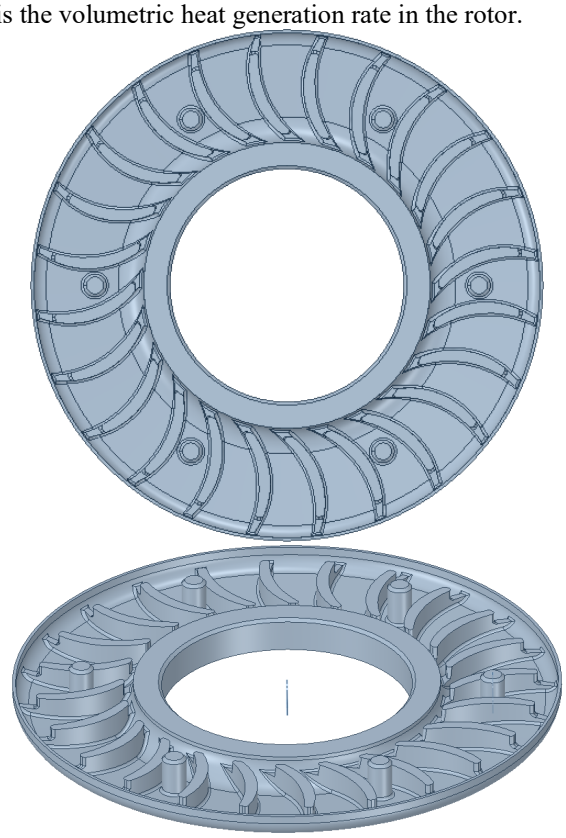

Fig. 2. Impeller fan design

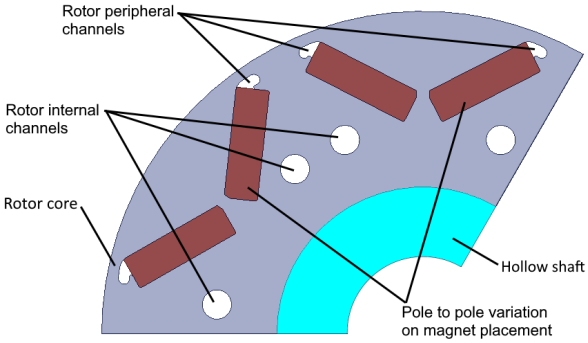

Fig. 3. 120 kW rotor lamination geometry

The variable temperature field on the cooled surface of the material $T(r, z, \tau)$ obtained as a result of solving (1) should meet the boundary conditions [12, 13]. They are written in the form of Fourier's law:

$$\dot{q}(r,\tau)=h(r,\tau)\cdot(T_s-T_p), \qquad (2)$$

where $\dot{q}$ is the heat flux density; $h(r, \tau)$ is the heat transfer coefficient; T_s is the surface temperature; T_p is the ambient temperature.

A two-dimensional axisymmetric thermal conductivity is assumed, in which heat exchange with the coolant occurs

only on one of the cylinder's front surfaces. The advantage of using formulas based on dimensionless analysis is that any gas or liquid can be used, even if the original formula was developed for a specific liquid [14, 15].

For natural convection, the typical form of convective correlation is:

$$Nu = a(GrPr)^b. \quad (3)$$

For forced convection the typical form of the convection correlation is:

$$Nu = a(Re)^b(Pr)^c. \quad (4)$$

where Nu is the dimensionless Nusselt number; a, b, c are the constants given in the correlation; Gr is the dimensionless Grashof number; Re is the dimensionless Reynolds number; Pr is the dimensionless Prandtl number. Also:

$$Re = \rho v L / \mu; \quad (5)$$

$$Gr = \beta G \Delta T \rho^2 L^3 / \mu^2; \quad (6)$$

$$Pr = c_p \mu / k; \quad (7)$$

$$Nu = hL / k, \quad (8)$$

where ρ is the fluid density; v is the fluid velocity; L is the characteristic length of the surface; μ is the fluid dynamic viscosity; β is the coefficient of cubical expansion, $1/(273+T_{FLUID})$; G is the gravitational force of attraction; ΔT is the delta temperature of surface-fluid; c_p is the fluid specific heat capacity; k is the fluid thermal conductivity.

The quantity Re is used to evaluate laminar or turbulent flow in a system with forced convection. The product of $GrPr$ is used in systems with natural convection. Ultimately, we are interested in the parameter h.

Heat transfer in natural convection depends primarily on the temperature difference between the vessel (in our case, the shaft) and the liquid (oil), as well as on the properties of the liquid. Forced convection depends primarily on the speed of the liquid and its properties, and only secondarily on the temperature, since the properties of the liquid depend on the temperature. Mixed heat transfer (h_{MX}), caused by a combination of natural (h_{NAT}) and forced (h_{FRC}) convection, is estimated using the formula [16, 17]:

$$h_{MX}^3 = h_{FRC}^3 \pm h_{NAT}^3, \quad (9)$$

where the motor rotation orientation determines the «±» sign used, a «+» sign for assisting and transverse flow and a «–» sign for opposing flows.

Table 1 shows the values of the coefficients a and b for laminar and turbulent flow also as the $GrPr$ product at which the transition to turbulent flow occurs for a smooth horizontal inner shaft surface.

Table 1

Correlation coefficients for natural convection

$GrPr$ laminar to turbulent	a, laminar	b, laminar	a, turbulent	b, turbulent
10^9	0.525	0.25	0.129	0.33

In case of smooth inner surface of the shaft, we can use the following correlations for the flow [17, 19, 20]:

- for the laminar flow ($(Re < 5 \cdot 10^5)$ and $(0.6 < Pr < 50)$):

$$Nu = 0.664(Re)^{0.5}(Pr)^{0.33}; \quad (10)$$

- for the turbulent flow ($(Re > 5 \cdot 10^5)$):

$$Nu = [0.037(Re)^{0.8} - 871](Pr)^{0.33}. \quad (11)$$

The heat transfer coefficient h can be calculated as:

$$h = \frac{\rho c_p v D}{4L}(1 - e^{-m}); \quad m = 0.1448 \frac{L^{0.946}}{D^{1.16}} \cdot \left(\frac{k}{\rho c_p v} \right)^{0.214}, \quad (12)$$

where D is the hydraulic diameter, L is the axial length of the shaft.

To predict the thermal behavior of the motor and optimized motor temperatures computer modeling and thermal monitoring such as lumped parameter thermal network, finite element analysis (FEA) and computational fluid dynamics (CFD) are used. Numerical models simulate various operating conditions, providing a comprehensive understanding of the thermal behavior of the motor. This predictive method allows for the identification of hot spots and, therefore, the optimization of the cooling system to prevent overheating.

The effect of end windings cooling for the machine under study was investigated using a 3D finite element method (FEM) thermal model in [18]. The paper compares the traditional method of cooling a machine with a hairpin winding with oil cooling of the end windings and stator stack cooling (SSC), and a new cooling concept, based on oil cooling of the end windings and direct oil cooling (DOC) of the slot conductors, which allows improving hairpin winding thermal management and increasing machine specific power.

The loss components distribution, thermal properties, and boundary coefficients applied to the developed models in [18] are shown in Tables 2, 3. The simulation results are shown in Fig. 4–7.

Table 2

Loss components distribution in machines with different cooling arrangements at different loads [18]

Parameter	SSC, 96 N·m	SSC, 48 N·m	DOC, 96 N·m	DOC, 48 N·m
Layer 1 losses	780 W	238 W	864 W	256 W
Layer 2 losses	596 W	184 W	686 W	204 W
Layer 3 losses	500 W	153 W	593 W	174 W
Layer 4 losses	434 W	131 W	529 W	153 W
Layer 5 losses	393 W	117 W	489 W	139 W
Layer 6 losses	375 W	110 W	471 W	133 W
End windings losses	839 W	251 W	1063 W	281 W
Stator core losses	2596 W	1576 W	2596 W	1576 W
Rotor core losses	144 W	81 W	144 W	81 W
Efficiency	0.946	0.946	0.942	0.945

Table 3

Thermal properties and boundary coefficients applied in the model [18]

Parameter	Value
Copper thermal conductivity	398 W/(m·K)
Stator core thermal conductivity	30 W/(m·K)
Rotor core thermal conductivity	30 W/(m·K)
HTC on the surface between end winding and oil flow	100 W/(m^2·K)
HTC on the surface between slot conductor and oil flow	500 W/(m^2·K)
HTC on the surface between stator stack and oil flow	500 W/(m^2·K)
Average oil temperature	60 °C

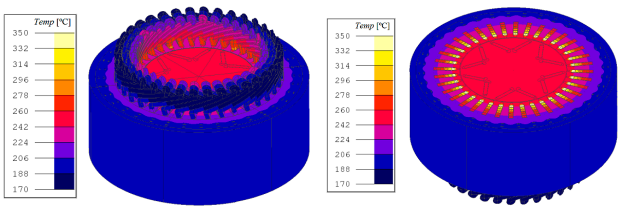

Fig. 4. Temperature distribution in 3D FEM model of the machine with oil cooling of the end windings and SSC at 12000 rpm, 96 N·m

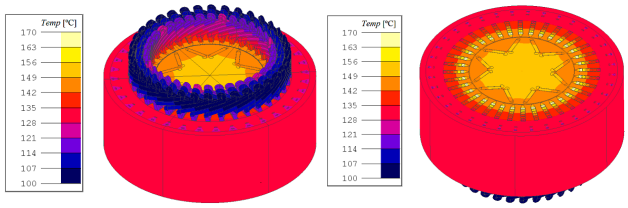

Fig. 5. Temperature distribution in 3D FEM model of the machine with oil cooling of the end windings and SSC at 12000 rpm, 48 N·m

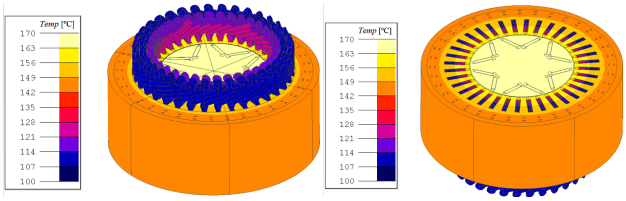

Fig. 6. Temperature distribution in 3D FEM model of the machine with oil cooling of the end windings and DOC at 12000 rpm, 96 N·m

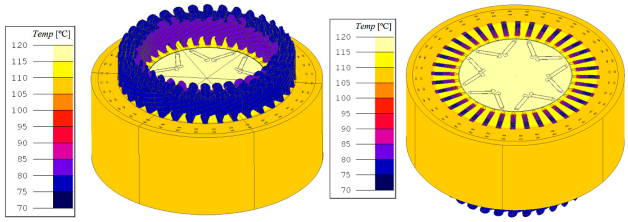

Fig. 7. Temperature distribution in 3D FEM model of the machine with oil cooling of the end windings DOC at 12000 rpm, 48 N·m

According to the simulation results obtained in [18], the PMSM with DOC has only 0.1 % lower efficiency at 48 N·m than the PMSM with SSC. This load is the maximum continuous operating range of the PMSM with standard winding. However, PMSM with DOC can obtain much higher continuous operating loads without the risk of being overheated due to more effective cooling.

The models used in [18] did not take into account for rotor cooling and natural heat dissipation from the stator frame, since these had a negligible effect on the stator winding's cooling. Therefore, the combined oil-air rotor cooling of the 120 kW machines with DOC at a load of 96 N·m was isolated into a separate problem, which is solved in this work.

CFD was chosen for analysis of the behavior of fluid and its interactions with surfaces. CFD simulations of liquid and gas flows are based on the assumption of the presence of inlet and outlet zones through which the simulated medium (in our case, air) freely flows into and out of the studied domain. Since the stator cavity in our case is sealed (there are no inlet or outlet zones), the thermal task of the proposed air cooling of the rotor, in general, appears to be unsolvable from the point of view of machine logic.

Therefore, the task was divided into 4 successive steps, in which the inlet and outlet zones swapped places at each step.

Step 1. The airflow inside the rotor channels and impeller cavity were simulated. All other parts of the model except the air domain and the front air volume were not considered. Inlet and outlet zones are the outer walls of the front air volume.

Step 2. The obtained values of airflow velocities and pressures were added to the laminate model. The thermal influence from the stator and the cold shaft was taken into account. Inlet and outlet zones – internal and external channels of the rotor.

Step 3. The values of airflow velocities, pressures and temperatures obtained in the previous Step were added to the frontal air volume. The thermal influence of the stator walls, cold shaft and front bearing shield on the frontal air volume was considered. Inlet and outlet zones – external and internal rotor channels.

Step 4. The refined values of airflow velocities, pressures and temperatures were added from the previous Step to the rotor model with the added rear air volume. In addition to the thermal influence from the stator and the cold shaft, the thermal influence from the rear bearing shield was also taken into account. Inlet and outlet zones – internal and external channels of the rotor.

The task statement diagram is shown in Fig. 8. Thermal properties and coefficients applied in the boundary regions of the 3D CFD model are listed in Table 4. The boundary conditions and the volumetric heat generation rate q''' in the rotor of the proposed design were obtained based on [18, 21] results:

$$q''' = P_{loss} / V_r = 144 \text{ W} / 0.000507 \text{ m}^3 \approx 284000 \text{ W/m}^3, \quad (13)$$

where P_{loss} is the total rotor core losses (Table 2); V_r is the specified rotor volume.

The computational mesh was generated automatically from combined tetrahedral and polyhedral elements.

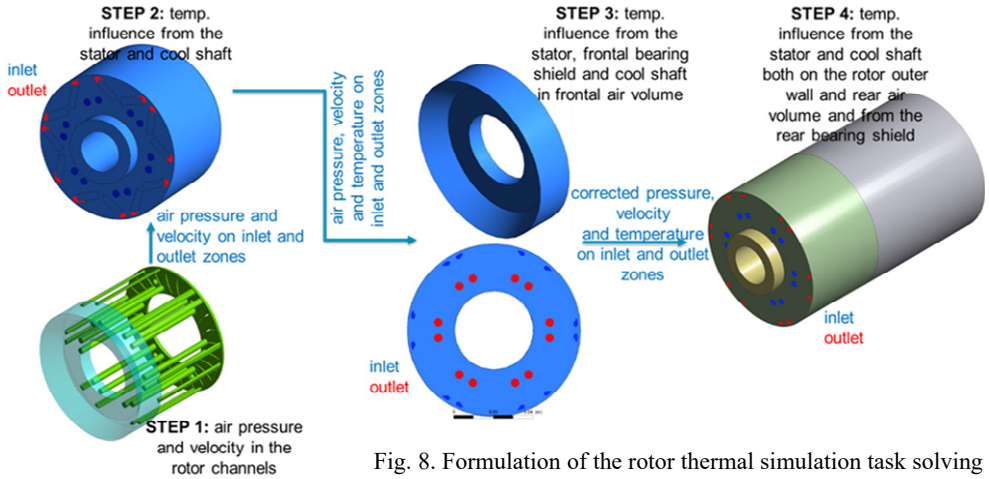

Fig. 8. Formulation of the rotor thermal simulation task solving

Table 4

The materials thermal properties and coefficients applied in the boundary regions

Parameter	Value
Rotor core steel thermal conductivity	23 W/(m K)
Shaft steel thermal conductivity	45 W/(m K)
Impeller aluminum thermal conductivity	200 W/(m K)
Magnets thermal conductivity	9 W/(m K)
HTC on the surface between channels in rotor core and air flow	25 W/(m^2 K)
HTC on the surface between bearing shields and air volumes	25 W/(m^2 K)
HTC on the surface between impeller and rear air volume	65 W/(m^2 K)
HTC on the surface between stator and air volumes	25 W/(m^2 K)
Heat generation rate in rotor	284000 W/m^3
Average bearing shields surface temperature	60° C, stable

Results. The geometry for CFD simulation of the air flow inside the rotor and the frontal air volume (Step 1) is shown in Fig. 9.

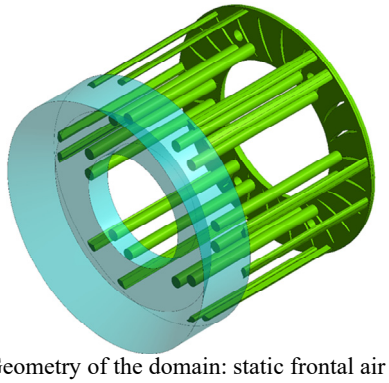

Fig. 9. Geometry of the domain: static frontal air volume (transparent blue) and rotating air domain (green)

CFD simulations at a rotation speed of 12000 rpm showed that the impeller creates clear zones of negative air pressure along the internal circuit and positive air pressure along the external circuit, while the internal and external channels are completely located inside the negative and positive pressure zones, respectively. As can be seen from the results obtained (Fig. 10), the internal channels of the rotor lie in defined zones of negative pressure in the range of 0.142–0.506 kPa, and the external channels of the rotor lie in zones of positive pressure in the range of 0.404–0.951 kPa. Thus, the pressure difference of the airflow between the internal and external channels of the rotor is 0.546–1.457 kPa, which makes pumping air through the rotor channels and the impeller possible.

In Fig. 11 it can be seen that at a rotor and impeller rotation speed of 12000 rpm in the internal channels (air suction) and in the external channels (air pumping out), it is possible to obtain stable flows with an average speed in the range of 20–30 m/s.

The calculated average flow velocities for known cross-sectional areas of the internal channels (12 channels with a cross-sectional area of 12.503 mm^2 each) and the external channels (12 channels with a cross-sectional area of 5.1265 mm^2 each) allow us to calculate the volumetric flow rate of air passing through these channels by (14) using Ansys Fluent built-in calculator:

$$Q = v \times S, \qquad (14)$$

where Q is the air volumetric flow rate, m^3/s, v is the air flow velocity, m/s, S is the cross-sectional area of the flow, m^2.

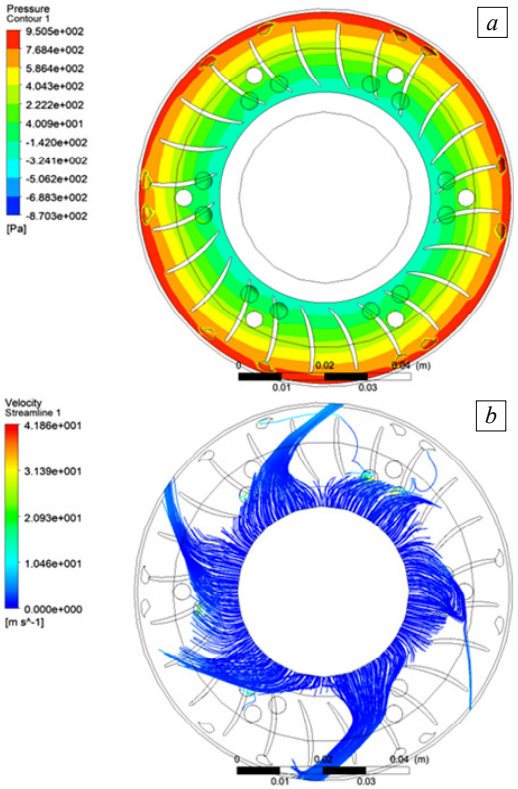

Fig. 10. The air pressure distribution (*a*) and the air velocity distribution in the frontal air volume during suction (*b*)

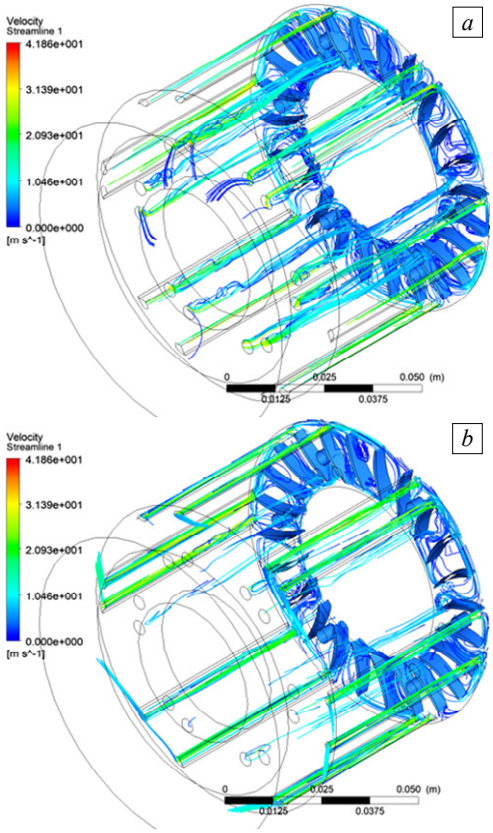

Fig. 11. The air velocity distribution in internal (*a*) and external (*b*) channels

The expected volumetric flow rate of air passing through internal channels is 0.003 m^3/s and the volumetric flow rate of air passing through external channels is 0.00258 m^3/s. As can be seen, the difference between the volumetric flow of air passing through the internal and

external channels is 14 %. The presence of such losses can be explained by inaccuracies in the simulation, uneven air flows through the rotor channels and local air turbulence occurring in the impeller. Considering the small volume of the frontal air volume (55300 mm^3 or 0.0000553 m^3), we can conclude that at the rotor rotation speed of 12000 rpm air from this cavity will be pumped through the rotor channels about 50 times per second.

Shaft cooling simulations were provided with Mobil EV Cool Drive 303 oil for different values of the oil flow rates and oil inlet temperatures (Fig. 12). All further simulations were performed at a rotor speed of 12000 rpm.

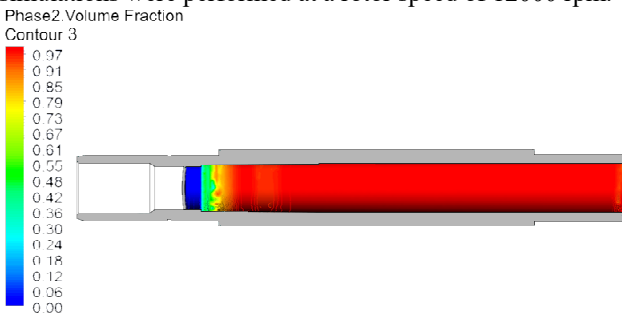

Fig. 12. Cross-section of oil volume fraction with 0.14 m/s inlet velocity (mass flow rate 0.24 l/min) at 12000 rpm rotation speed

In Table 5 results of the shaft inner surface heat transfer coefficient calculations are shown.

Table 5

Oil-inner shaft surface heat transfer coefficient

Oil-inner shaft surface HTC h, W/(m^2 K)			
Oil flow rate q, l/min	Oil inlet temperature θ_{oil}, °C		
	30	45	60
0.12	194.6	194.8	195.2
0.24	196.7	198.2	197.8
0.36	218.2	219.2	222.8

As can be seen (Fig. 13), considering the dynamic properties of the selected oil, the key factor affecting the value of the HTC is the value of the volumetric flow rate of oil, while the initial temperature of the oil affects this parameter insignificantly. In further simulations, the average value of h = 204 W/(m^2 K) was used.

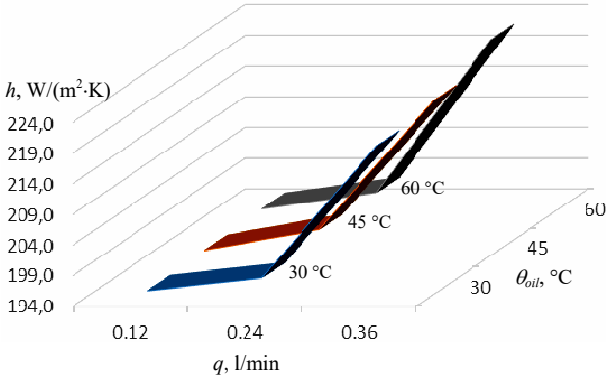

Fig. 13. Shaft inner surface HTC rates

Figure 14 shows the thermal behavior of the air domain in the rotor channels and the cavity of the impeller and the shaft after corrected rotor thermal analysis (Step 4). As can be seen, warm air enters the internal channels (inlet zones) and is cooled as it moves through the channels along the shaft, and then exits through the outer channels (the outlet zones) already cooled. The shaft is taking heat along its length from the front edge to the rear, where it borders the impeller. Thus, it can be concluded that air temperatures are taken out by the shaft through the body of the rotor laminate.

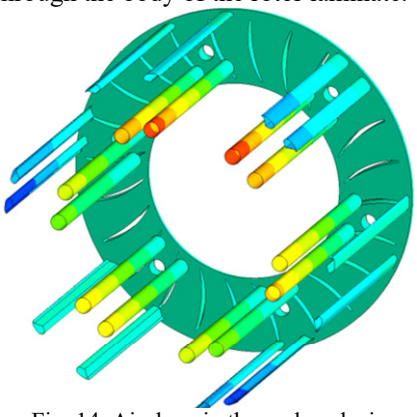

Fig. 14. Air domain thermal analysis

Figure 15 shows temperature distribution patterns along the frontal and the rear faces of the rotor. It can be seen that the approximate temperature in the middle zone of the rotor is in the range of 80 °C, and the outer peripheral zone cools even more. In the very narrow areas between the outer outlet channels, temperatures of 64 °C are reached. In Fig. 15,*b*, the rear face of the rotor is shown. As can be seen, it cools more efficiently than the frontal face (Fig. 15,*a*), and the temperature spots on it have lower values than on the frontal one.

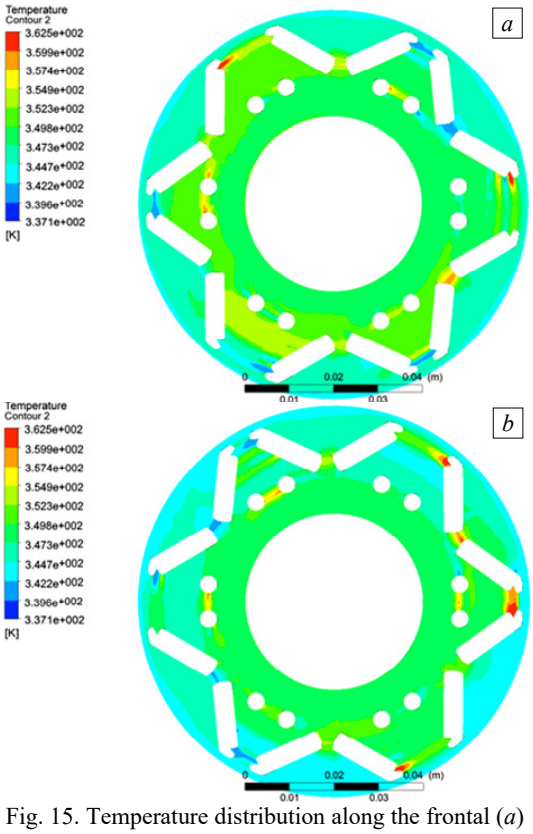

Fig. 15. Temperature distribution along the frontal (*a*) and the rear (*b*) faces of the rotor

Figure 16 shows a picture of the temperature distribution in the PMs. As can be seen, the PMs heat up unevenly. This could be explained by the asymmetry of the impeller, the asymmetry and unequal airflows it creates, as well as the asymmetry of the rotor itself and the location of the magnets in it, and also the low thermal conductivity of

the magnets specified in the model. The peak temperatures achieved in the PMs do not exceed 64 °C.

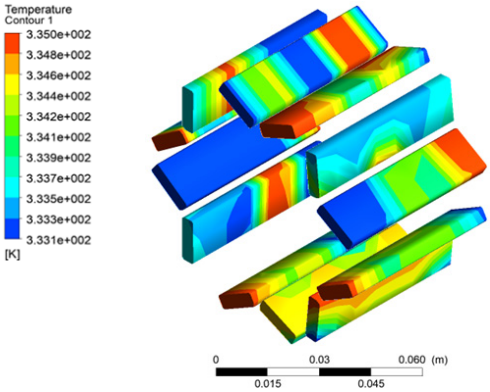

Fig. 16. Temperature distribution in the PMs

Figure 17 shows the effect of air circulation in the rotor channels created by an impeller fan (with and without the presence of the air domain in the simulation system) on the temperature distribution in the «shaft-rotor» system.

As can be seen from the obtained results, including the Air domain in the simulation system (air circulates in both directions due to the pressure difference between the outer and inner channels inside the rotor) reduces rotor heating, including in the PM V zone. The main achievement is the avoidance of high-temperature fields (hot spots) concentrated in the outer zone of the rotor. Thus, the creation of bidirectional air flows generated by the impeller fan simultaneously with the oil circulation inside the hollow shaft not only reduces but also more evenly distributes temperatures within the rotor.

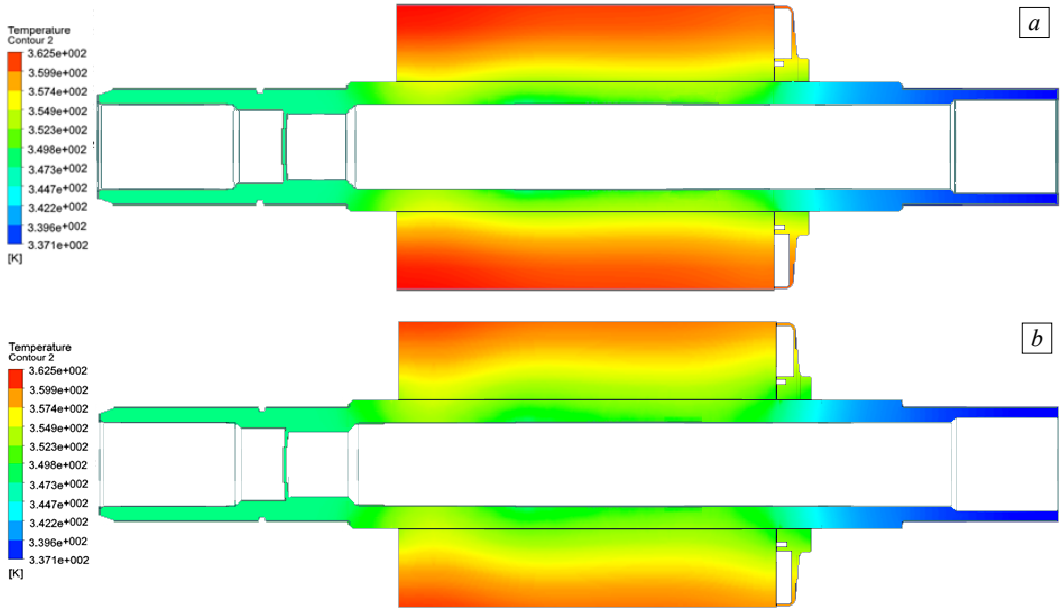

Fig. 17. Cross-section of temperature distribution across the shaft and rotor at 12000 rpm speed rotation: *a* – air circulation disabled; *b* – air circulation enabled

Conclusions. As can be seen from the obtained results, the presence of bidirectional air circulation inside the rotor lamination channels, created by the impeller fan, with simultaneous circulation of oil in the hollow shaft, allows for the redistribution and reduction of the rotor core temperature with a virtually unchanged hollow shaft temperature.

The key factor affecting the value of the heat transfer coefficient between hollow shaft inner surface and oil inside it is the value of the volumetric flow rate of oil, while the initial temperature of the oil affects this parameter insignificantly. Further development involves studying the effect of the rotation speed of the hollow shaft on the value of the heat transfer coefficient.

As stated above, the CFD simulations of the thermal distribution in the rotor and the analysis of the possibility of its cooling by bidirectional air flows created by the impeller fan were carried out taking into account the assumption that the temperature emanating from the front and rear bearing shields, as well as the temperature of the oil in the shaft, are constant and stable.

Possible further studies include the following:

- clarification of temperature indicators of bearing units and their possible influence on temperatures in the rotor;
- study of the influence of rotation speed (and, therefore, air and oil flow intensity) on the temperature in the rotor;
- study of the influence of oil volume flow and its inlet temperature in the hollow shaft on the shaft temperature and temperature distribution in the rotor as a whole;
- study of vibrations from the impeller;
- study of the power losses in the impeller and its efficiency;
- further comprehensive FEA/CFD analysis of the traction electric motor thermal state, taking into account both the stator cooling and the proposed rotor cooling method.

Acknowledgements. This work was partly supported by EU VOLTCAR project funded by the European Union under Grant Agreement no. 101096557. Views and opinions expressed are however those of the author(s) only and do not necessarily reflect those of the European Union or the European Climate, Infrastructure and Environment Executive Agency (CINEA). Neither the European Union nor the granting authority can be held responsible for them.

Conflict of interest. The authors declare that they have no conflicts of interest.

REFERENCES

1. Usman A., Saxena A. Technical Roadmaps of Electric Motor Technology for Next Generation Electric Vehicles. *Machines*, 2025, vol. 13, no. 2, art. no. 156. doi: https://doi.org/10.3390/machines13020156.

2. Biot-Monterde V., Navarro-Navarro A., Zamudio-Ramirez I., Antonino-Daviu J., Osornio-Rios R.A., Ruiz-Sarrió J.E. Automatic classification of stator asymmetries and insulation thermal damages in induction motors, applying persistence spectrum and a convolutional neural network to the stray-flux signals. *2023 IEEE 32nd International Symposium on Industrial Electronics (ISIE)*, 2023, pp. 1-6. doi: https://doi.org/10.1109/ISIE51358.2023.10227984.

3. Sun W., Gao F. Failure Analysis of Irreversible Demagnetization of Permanent Magnet Synchronous Motor. *2024 11th International Forum on Electrical Engineering and Automation (IFEEA)*, 2024, pp. 761-764. doi: https://doi.org/10.1109/IFEEA64237.2024.10878522.

4. Neusues S., Binder A. Post rotor-fault operation of a Ferrite Magnet assisted Synchronous Reluctance Motor. *2020 International Conference on Electrical Machines (ICEM)*, 2020, pp. 2335-2341. doi: https://doi.org/10.1109/ICEM49940.2020.9271011.

5. Fu J., Li H., Sun X., He T., Zhang G., Wei C. Multi-physics simulation modeling and energy flow characterization of thermal management system for a sport utility vehicle under high-temperature conditions. *Energy*, 2025, vol. 316, art, no. 134653. doi: https://doi.org/10.1016/j.energy.2025.134653.

6. Malik M.A.I., Kalam M.A., Ikram A., Zeeshan S., Raza Zahidi S.Q. Energy transition towards electric vehicle technology: Recent advancements. *Energy Reports*, 2025, vol. 13, pp. 2958-2996. doi: https://doi.org/10.1016/j.egyr.2025.02.029.

7. Dan D., Zhao Y., Wei M., Wang X. Review of Thermal Management Technology for Electric Vehicles. *Energies*, 2023, vol. 16, no. 12, art. no. 4693. doi: https://doi.org/10.3390/en16124693.

8. Wu J., Shan L., Peng G., Wang R., Zhang W., Tong X., Shen L. A Review of Motor Drive Thermal Management System for Electric Vehicles. *2022 7th International Conference on Power and Renewable Energy (ICPRE)*, 2022, pp. 551-556. doi: https://doi.org/10.1109/ICPRE55555.2022.9960497.

9. Gronwald P.-O., Kern T.A. Traction Motor Cooling Systems: A Literature Review and Comparative Study. *IEEE Transactions on Transportation Electrification*, 2021, vol. 7, no. 4, pp. 2892-2913. doi: https://doi.org/10.1109/TTE.2021.3075844.

10. Bourgault A.J., Roy P., Ghosh E., Kar N.C. A Survey of Different Cooling Methods for Traction Motor Application. *2019 IEEE Canadian Conference of Electrical and Computer Engineering (CCECE)*, 2019, pp. 1-4. doi: https://doi.org/10.1109/CCECE.2019.8861611.

11. Gundabattini E., Kuppan R., Solomon D.G., Kalam A., Kothari D.P., Abu Bakar R. A review on methods of finding losses and cooling methods to increase efficiency of electric machines. *Ain Shams Engineering Journal*, 2021, vol. 12, no. 1, pp. 497-505. doi: https://doi.org/10.1016/j.asej.2020.08.014.

12. Li X., Zhao X., Zhang Z., Avelin A., Liu S., Li H. Selecting cooling methods for electric motors. *Applied Thermal Engineering*, 2025, vol. 274, art. no. 126554. doi: https://doi.org/10.1016/j.applthermaleng.2025.126554.

13. Cengel Y.A., Cimbala J.M., Ghajar A.J. *Fundamentals of Thermal-Fluid Sciences. 6th edition*. McGraw Hill, 2022. 977 p.

14. Dheivanai R., Prasanth B., Karthikeyan G. Evaluation and Simulation of Oil-based Direct Cooling System in Series DC Motors for Electric Vehicle Applications. *Iranian Journal of Science and Technology, Transactions of Electrical Engineering*, 2025. doi: https://doi.org/10.1007/s40998-025-00833-2.

15. Szajding A., Gołdasz A., Telejko T. The influence of coolant velocity on the local heat transfer coefficient during steel quenching. *Computer Methods in Material Science*, 2020, vol. 20, no. 4, pp. 157-164. doi: https://doi.org/10.7494/cmms.2020.4.0737.

16. Zhang T., Yao J., Liao S., Liu X., Xu Y., Yang S. Cooling enhancement of permanent magnet synchronous motor coupled with heat pipes for electric vehicle. *Applied Thermal Engineering*, 2025, vol. 279, art. no. 127572. doi: https://doi.org/10.1016/j.applthermaleng.2025.127572.

17. Milykh V.I. Numerical-field analysis of active and reactive winding parameters and mechanical characteristics of a squirrel-cage induction motor. *Electrical Engineering & Electromechanics*, 2023, no. 4, pp. 3-13. doi: https://doi.org/10.20998/2074-272X.2023.4.01.

18. Petrov I., Martikainen I., Poutiainen I., Rangwala J., Pyrhönen J. Hairpin Winding with Direct Oil Cooling. *2024 International Conference on Electrical Machines (ICEM)*, 2024, pp. 1-7. doi: https://doi.org/10.1109/ICEM60801.2024.10700210.

19. Ibrar A., Ahmad S., Safdar A., Haroon N. Efficiency enhancement strategy implementation in hybrid electric vehicles using sliding mode control. *Electrical Engineering & Electromechanics*, 2023, no. 1, pp. 10-19. doi: https://doi.org/10.20998/2074-272X.2023.1.02.

20. Bergman T.L., Lavine A.S., Incropera F.P., DeWitt D.P. *Introduction to Heat Transfer. 6th edition.* John Wiley & Sons, Inc., 2011. 1040 p.

21. Milykh V.I. Theory and practice of numerical-field analysis and refinement of electromagnetic and energy parameters in the designs of three-phase induction motors. *Electrical Engineering & Electromechanics*, 2026, no. 1, pp. 3-14. doi: https://doi.org/10.20998/2074-272X.2026.1.01.

Received) 13.11.2025
Accepted 15.01.2026
Published 02.05.2026

S. Shlyk[1]*, PhD, Associate Professor,*
J. Pyrhönen[2]*, D.Sc. (Tech.), Professor,*
I. Petrov[2]*, D.Sc. (Tech.), Associate Professor,*
M. Parviainen[2]*, Junior Researcher,*
I. Martikainen[2]*, Project Engineer,*
A. Suikki[3]*, Senior Mechanical Engineer,*
J. Pippuri-Mäkeläinen[4]*, D.Sc. (Tech.), Professor,*
M. Zagirnyak[1]*, D.Sc. (Tech.), Professor,*
[1] Kremenchuk Mykhailo Ostrohradskyi National University,
20, Universytetska Str., Kremenchuk, 39600, Ukraine,
e-mail: mzagirn@gmail.com (Corresponding Author).
[2] Lappeenranta-Lahti University of Technology LUT,
34, Yliopistonkatu, Lappeenranta, 53850, Finland.
[3] Danfoss Editron Oy,
44, Lentokentäntie, Lappeenranta, 53600, Finland,
[4] VTT Technical Research Centre of Finland Ltd,
3, Vuorimiehentie, Espoo, FI-02044, Finland.

How to cite this article:
Shlyk S., Pyrhönen J., Petrov I., Parviainen M., Martikainen I., Suikki A., Pippuri-Mäkeläinen J., Zagirnyak M. Possibility of cooling the rotor of an electric traction motor by bidirectional air flows. *Electrical Engineering & Electromechanics*, 2026, no. 3, pp. 26-33. doi: https://doi.org/10.20998/2074-272X.2026.3.04